Hindawi Publishing Corporation
Journal of Nanomaterials
Volume 2015, Article ID 857506, 6 pages
http://dx.doi.org/10.1155/2015/857506

Research Article

Synthesis and Photocatalytic Activity of Ag_3PO_4 Triangular Prism

Pengyu Dong,[1] Yan Hao,[2] Peiyang Gao,[2] Entian Cui,[1] and Qinfang Zhang[1]

[1]*Key Laboratory for Advanced Technology in Environmental Protection of Jiangsu Province, Yancheng Institute of Technology, Yancheng 224051, China*
[2]*School of Materials Engineering, Yancheng Institute of Technology, Yancheng 224051, China*

Correspondence should be addressed to Pengyu Dong; dongpy11@gmail.com

Received 18 November 2014; Accepted 4 January 2015

Academic Editor: Cao Yuebin

Ag_3PO_4 triangular prism was synthesized by a facile chemical precipitation approach by simply adjusting external ultrasonic condition. The as-synthesized Ag_3PO_4 triangular prism was characterized by X-ray diffraction pattern (XRD), field emission scanning electron microscopy (SEM), fourier transform infrared (FTIR) spectra, and ultraviolet-visible diffuse reflectance (UV-vis DRS) absorption spectra. The photocatalytic activity of Ag_3PO_4 triangular prism was evaluated by photodegradation of organic methylene blue (MB), rhodamine B (RhB), and phenol under visible light irradiation. Results showed that Ag_3PO_4 triangular prism exhibited higher photocatalytic activity than N-doped TiO_2 and commercial TiO_2 (P25) under visible light irradiation.

1. Introduction

Photocatalysis technology is considered as an efficient, stable, and environmentally friendly method for controlling environmental pollutions [1]. In the past years, the discovery of new efficient visible-light-driven photocatalysts attracts much attention. It is noted that a breakthrough on visible-light-driven photocatalysts was made by Yi et al.'s research team, who reported the use of Ag_3PO_4 as an active visible-light-driven photocatalyst for oxidation of water and photodecomposition of organic compounds [2]. This research finding is considered as a breakthrough in the field of visible-light active photocatalysts. Hence, investigation of the basic principles and application of Ag_3PO_4 photocatalyst is a hot topic. Up to now, various methods have been proposed to further enhance the visible-light-driven photocatalytic activity. One of the methods is the coupling of Ag_3PO_4 with other semiconductors or noble metals to promote the charge separation efficiency of Ag_3PO_4 and then enhancing of the photocatalytic activity. Some composite samples such as Ag_3PO_4/TiO_2 [3], $AgBr@Ag_3PO_4/Fe_3O_4$ [4], Ag_3PO_4/graphene oxide [5], $Ag_3PO_4/TiOF_2$ [6], Ag_3PO_4/Ag [7], Ag_3PO_4/ZnO [8], Ag_3PO_4/BiOCl [9], Ag_3PO_4/reduced graphite oxide sheets [10], and g-C_3N_4/Ag_3PO_4 [11] have recently been developed to enhance the photocatalytic activity of Ag_3PO_4. Another method is the synthesis of Ag_3PO_4 with various new morphologies. In addition, it is known that the morphologies and microstructures of functional materials affect the physical and chemical properties [12, 13]. The morphology control of photocatalysts was considered to be one of the most promising avenues to improve the photocatalytic properties [14]. Therefore, further studies on Ag_3PO_4 crystals with new morphologies and structures will be of great value. In recent years, some morphologies of Ag_3PO_4 have been reported [15–21]. For example, Bi et al. fabricated the single-crystalline Ag_3PO_4 rhombic dodecahedrons with {110} facets exposed and cubes bounded entirely by {100} facets, and they found that both of these samples exhibited higher photocatalytic activity than the microsized spherical Ag_3PO_4 particles [15]. Our research group prepared Ag_3PO_4 nanorods with enhanced photocatalytic activity [16]. Wang et al. synthesized the tetrahedral Ag_3PO_4 crystals exposed with {111} facets [17]. Liang et al. synthesized hierarchical Ag_3PO_4 porous microcubes with enhanced photocatalytic

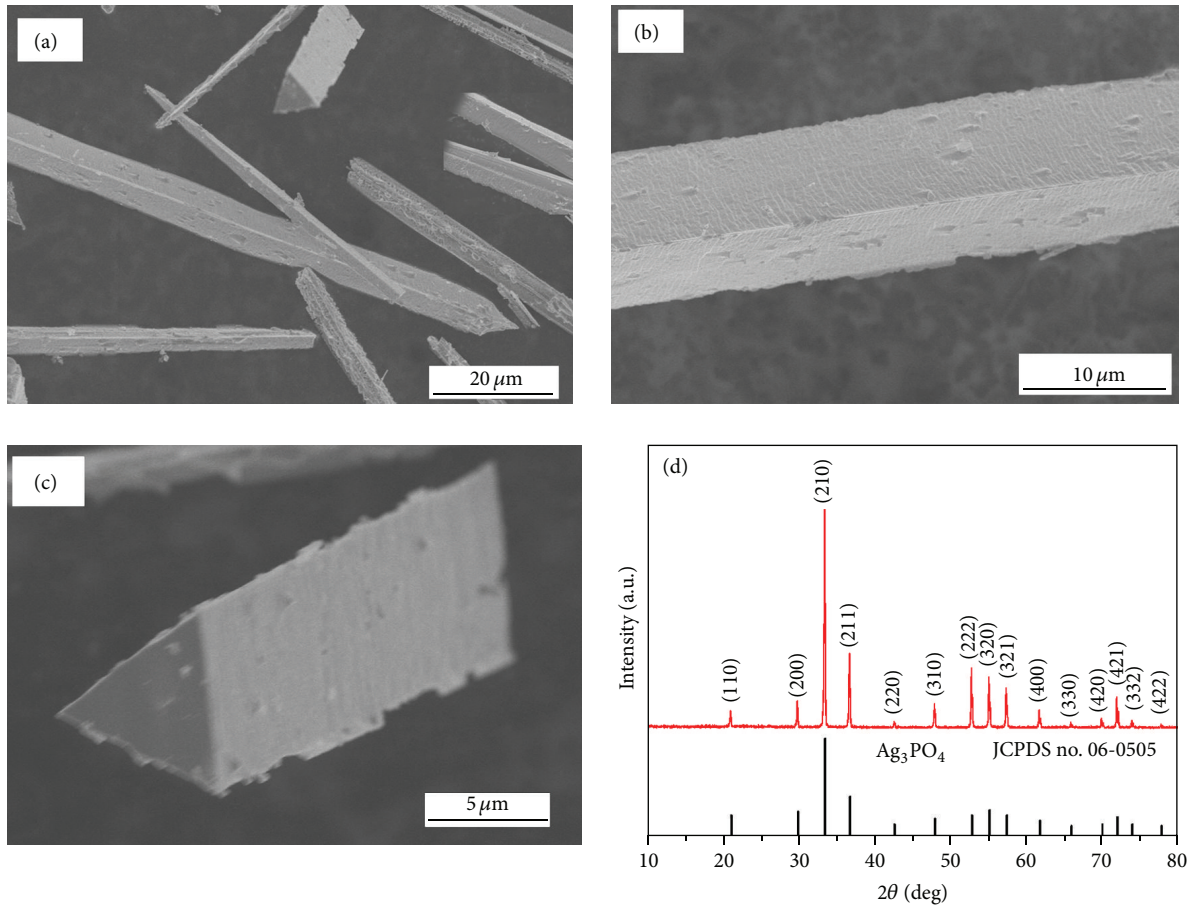

Figure 1: (a)–(c) SEM images and (d) XRD pattern of as-prepared Ag_3PO_4 sample.

property [18]. Up to now, synthesis of Ag_3PO_4 crystals with novel morphologies or microstructures is still an important and challenging research field.

To the best of our knowledge, there is no research on the synthesis of Ag_3PO_4 triangular prism. Herein, we controllably prepared Ag_3PO_4 triangular prism via a facile and efficient synthesis process in the mixture solvent of DMF and H_2O at room temperature. Meanwhile, the photocatalytic activity was investigated in this paper.

2. Experimental

In a typical preparation procedure, 10 mL of N,N-dimethylformamide (DMF) and 10 mL of deionized water (H_2O) were mixed together to form transparent solvent. Then, 3 mmol of $AgNO_3$ was dissolved into the mixture solvent. Subsequently, H_3PO_4 (1 mL, 85%) was added dropwise into the above solution under ultrasonic condition (ultrasonic reactor, KQ-100B, 40 kHz, 120 W/cm^2, Kunshan Co., China). After this process, the ultrasonic condition was maintained for 4 h. The obtained precipitation was separated by centrifuge and followed by washing with ethanol and deionized water for 3 times, respectively, to remove the DMF and other residues. Finally, the product was dried at 60°C. For comparison purpose, N-doped TiO_2 was synthesized by a reported method [22]. The commercial TiO_2 (P25) was purchased from Degussa.

X-ray diffraction (XRD) experiment was carried out with a D/max-2400 diffractometer (Rigaku, Japan) using Cu-Ka radiation. The morphologies of the sample were examined by scanning electron microscopy (SEM, Hitachi S-4800). Fourier transform infrared (FTIR) spectrum of the sample was recorded between 400 and 4000 cm^{-1} on a Nicolet NEXUS 670 FTIR spectrometer. Ultraviolet-visible diffuse reflectance (UV-vis DRS) absorption spectrum was measured using a Perkin Elmer 950 spectrometer, while $BaSO_4$ was used as a reference.

The photocatalytic activity of sample was measured by decomposition of methylene blue (MB) and rhodamine B (RhB) in a reactor at room temperature. In a typical process for degradation of a dye, 50 mg of photocatalyst was suspended in the dye solution (10 mg/L, 60 mL). Before irradiation, the suspensions were stirred in the dark for 60 min to ensure the establishment of adsorption-desorption equilibrium. A 350 W Xe lamp with a cutoff filter of 420 nm was employed for the visible-light irradiation source and positioned 20 cm away from the reactor to trigger the photocatalytic reaction. A certain volume of suspension was withdrawn at selected times for analysis. After recovering the photocatalyst by centrifugation, the concentration of dye

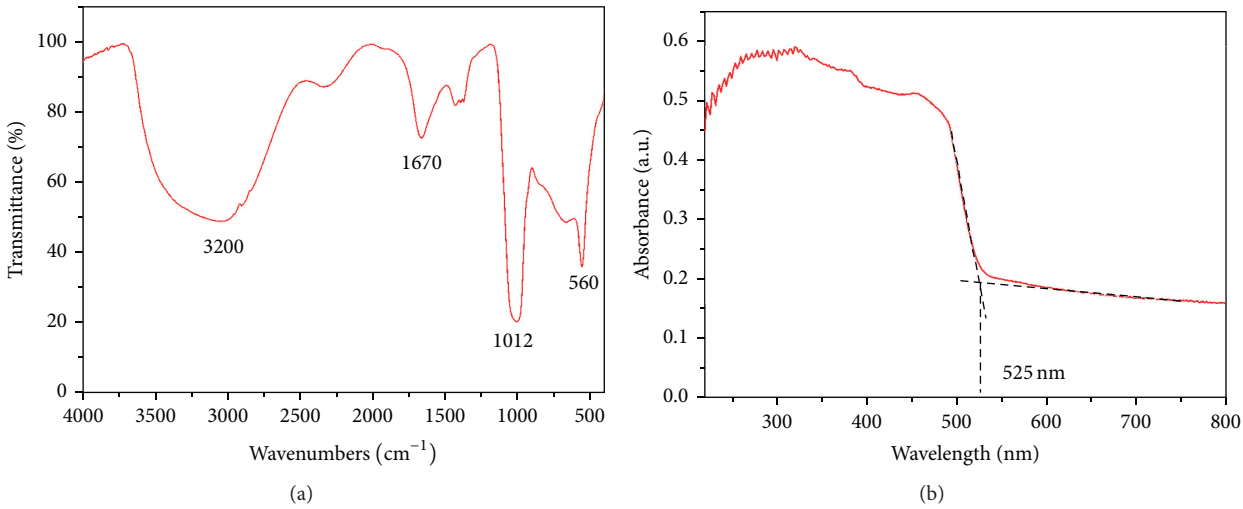

FIGURE 2: (a) FTIR spectrum of Ag_3PO_4 triangular prism in the regions of 4000–400 cm^{-1}, (b) UV-vis diffuse reflectance absorption spectrum of Ag_3PO_4 triangular prism.

solution was analyzed by measuring the light absorption of the clear solution at 664 nm (λ_{max} for MB solution) or 555 nm (λ_{max} for RhB solution) using a Perkin Elmer 950 spectrometer. The percentage of degradation was calculated by C/C_0. Here, C is the concentration of remaining dye solution at each irradiated time interval, while C_0 is the initial concentration. Furthermore, a colorless compound, phenol, was also chosen as a model pollutant since phenol shows no absorption in the visible region. The concentration of phenol solution was analyzed by measuring the light absorption of the clear solution at 270 nm (λ_{max} for phenol solution).

To test the stability of Ag_3PO_4 triangular prism, the cycling runs in photocatalytic degradation of MB in the presence of Ag_3PO_4 triangular prism were measured. After one cycle, the photocatalyst was filtrated and washed thoroughly with deionized water, and then fresh MB solution (10 mg/L) was added to the photocatalyst to begin the next cycling run. Five consecutive cycles were completed and each cycle lasted for 60 min.

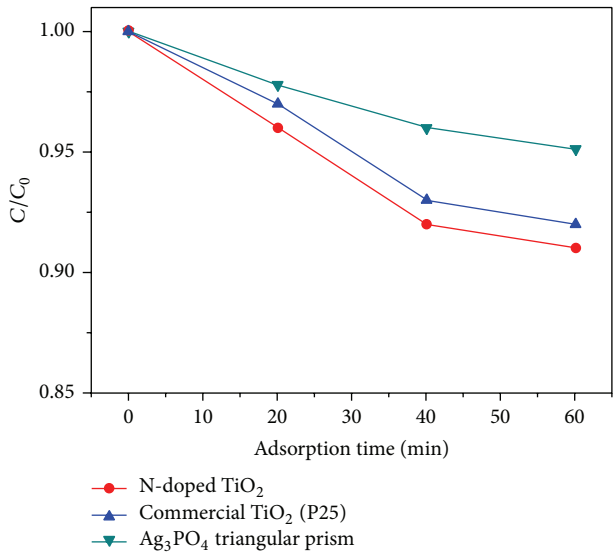

FIGURE 3: MB adsorption as a function of adsorption time over the as-prepared Ag_3PO_4 triangular prism, N-doped TiO_2, and commercial TiO_2 (P25) under a dark condition.

3. Results and Discussion

The SEM images of as-prepared sample were displayed in Figures 1(a)–1(c). It is observed that more than 80% of the product could be assigned to the triangular-prism-shaped morphology in this sample. Moreover, the lengths of bottom and chamfered edges are up to several micrometers. The XRD pattern of as-prepared triangular-prism-shaped sample was shown in Figure 1(d). All the diffraction peaks could be indexed to the cubic Ag_3PO_4 phase (JCPDS number 06-0505). Combining the SEM results, a conclusion that Ag_3PO_4 triangular prism was obtained can be drawn. The synthesis mechanisms of Ag_3PO_4 triangular prism could be explained as follows: the ultrasound assisted method could accelerate solid particles to high velocities via creating cavitation and shock waves, which leads to interparticle collision and effective fusion at the point of collision [23, 24]. This kinetic process speeds up the diffusion of Ag_3PO_4 nuclei in the reaction system, resulting in the formation of unique triangular-prism-shaped morphology, which can be attributed to the Ostwald ripening progress.

The chemical compositions of as-prepared Ag_3PO_4 triangular prism were examined by means of FTIR method. Figure 2(a) shows the FTIR spectrum of Ag_3PO_4 triangular prism. A strong and broad absorption around 3200 cm^{-1} and a sharp band at 1670 cm^{-1} are observed, which could be attributed to the stretching vibration of O–H and the bending vibration of H–O–H of residual water molecules, respectively. Besides that, two strong absorption bands are observed at 1012 and 560 cm^{-1}, which can be assigned to the molecular

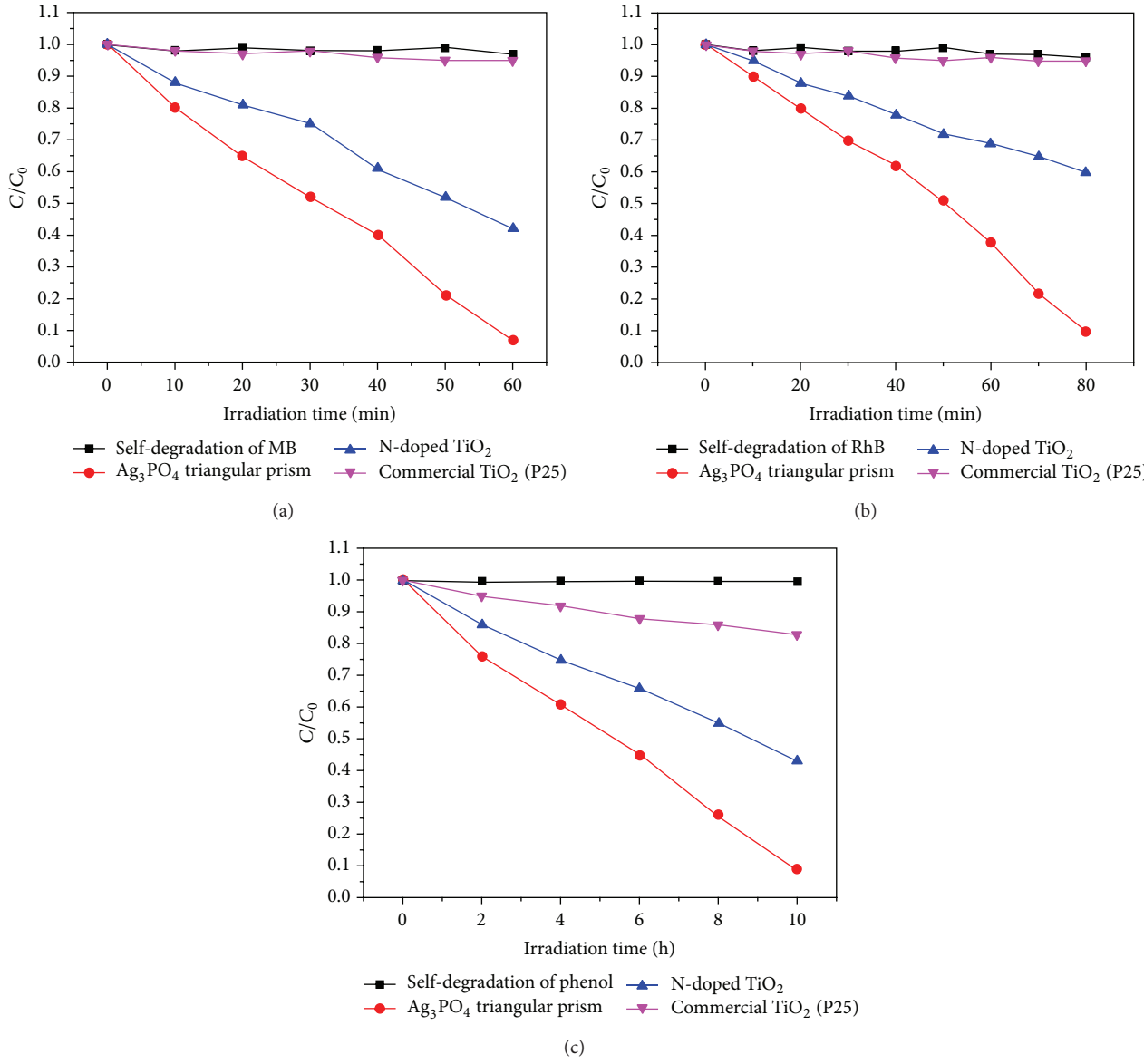

Figure 4: Variation of (a) MB, (b) RhB, and (c) phenol solution concentration against illumination time in the presence of Ag_3PO_4 triangular prism, N-doped TiO_2, and commercial TiO_2 (P25) under visible-light irradiation.

vibrations of phosphate (PO_4^{3-}) [25, 26]. This result confirms that there are no DMF molecules adsorbed on the surfaces of Ag_3PO_4 triangular prism. The UV-vis absorption spectrum of as-prepared Ag_3PO_4 triangular prism is displayed in Figure 2(b). It reveals that the absorption edge of Ag_3PO_4 triangular prism is around 525 nm, which means that it could strongly absorb a large part of visible light (400–525 nm).

Figure 3 shows the adsorption-desorption isotherms of as-prepared Ag_3PO_4 triangular prism, N-doped TiO_2, and commercial TiO_2 (P25) in the dark. It is found that most of the adsorption of dyes occur within 40 min, and the adsorption-desorption equilibrium can be achieved within 60 min. Moreover, it is observed that the adsorption affinity follows the order N-doped TiO_2 > commercial TiO_2 (P25) > Ag_3PO_4 triangular prism. Clearly, the Ag_3PO_4 triangular prism shows lower adsorption affinity for MB compared to the N-doped TiO_2 and commercial TiO_2 (P25), which could be associated with the size of samples. The size of Ag_3PO_4 triangular prism is around several micrometers, while the size of N-doped TiO_2 and commercial TiO_2 (P25) is about 20~50 nanometers. Larger size of Ag_3PO_4 triangular prism leads to the poor adsorption of MB molecules on the surfaces of Ag_3PO_4 triangular prism, resulting in the lower adsorption affinity.

The photocatalytic activity of samples was then investigated after reaching the adsorption-desorption equilibrium in the dark. Figure 4 shows the photocatalytic degradation behavior. From Figures 4(a) and 4(b), it can be seen that self-degradation of MB and RhB was not obvious under visible-light irradiation, indicating that MB and RhB can be used as

the targeted pollutants. It is noted that the percentage of photocatalytic degradation of MB for Ag_3PO_4 triangular prism, N-doped TiO_2, and commercial TiO_2 (P25) is 93%, 58%, and 5%, respectively. Accordingly, the percentage of photocatalytic degradation of RhB for Ag_3PO_4 triangular prism, N-doped TiO_2, and commercial TiO_2 (P25) is 90%, 40%, and 5%, respectively. Therefore, the percentage of photocatalytic degradation of MB and RhB for the samples follows the following order: Ag_3PO_4 triangular prism > N-doped TiO_2 > commercial TiO_2 (P25). This result clearly indicates that the Ag_3PO_4 triangular prism shows higher photocatalytic activity under visible-light irradiation, which could attribute to the strong visible-light absorption of Ag_3PO_4 triangular prism. In contrast, N-doped TiO_2 could absorb a small part of visible light, and commercial TiO_2 (P25) cannot make use of visible light because of a large band gap (3.2 eV). Since the MB and RhB dyes may absorb visible light, the sensitization possibility for samples should be considered. Then, the photocatalytic activity of the samples was also evaluated by colorless phenol degradation to ensure the visible-light photocatalytic activity and exclude the dye sensitization under visible light. The degradation of phenol with Ag_3PO_4 triangular prism, N-doped TiO_2, and commercial TiO_2 (P25) under visible-light irradiation was presented in Figure 4(c). It is clear that the concentration of phenol decreases with the irradiation time. Moreover, the Ag_3PO_4 triangular prism sample shows slightly higher photocatalytic activity for colorless phenol degradation compared to N-doped TiO_2 and commercial TiO_2 (P25).

The enhanced photocatalytic activity of Ag_3PO_4 triangular prism could be ascribed to the optical absorption property and unique electronic structure of Ag_3PO_4 crystals. Since the optical absorption edge of Ag_3PO_4 triangular prism is around 525 nm, the sample of Ag_3PO_4 triangular prism could strongly absorb a large part of visible light (400–525 nm). In addition, the highest valence band edge potential of Ag_3PO_4 crystals is 2.67 V (versus normal hydrogen electrode), which has strong driving force for photocatalytic degradation of pollutants [27].

The photocatalytic stability of Ag_3PO_4 triangular prism was shown in Figure 5. It is observed that the photocatalytic activity of Ag_3PO_4 triangular prism is decreased slowly in five successive experimental runs. This result indicates that the photocatalytic activity of Ag_3PO_4 triangular prism is unstable, which needs to be improved in the later study.

4. Conclusions

A new morphology, Ag_3PO_4 triangular prism, was successfully synthesized in the mixture solvent of DMF and H_2O under ultrasonic condition within 4 h. This synthetic method does not need the assistance of any hard/soft template. Although the Ag_3PO_4 triangular prism shows lower adsorption affinity for MB molecules, the photocatalytic results indicate that Ag_3PO_4 triangular prism shows enhanced photocatalytic activity compared with N-doped TiO_2 and commercial TiO_2 (P25). In addition, the photocatalytic stability of Ag_3PO_4 triangular prism needs to be further improved by various methods in the later study.

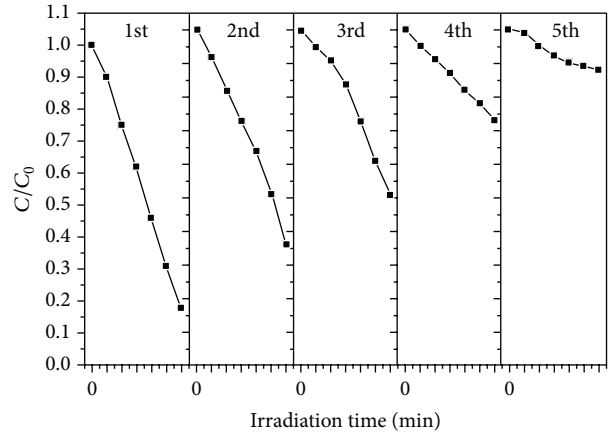

Figure 5: Repeated photocatalytic degradation of MB solution in the presence of Ag_3PO_4 triangular prism under visible-light irradiation.

Conflict of Interests

The authors declare that there is no conflict of interests regarding the publication of this paper.

Acknowledgments

This work is financially supported by the National Natural Science Foundation of China (Grants nos. 21403184 and 11204265), Natural Science Foundation of the Jiangsu Higher Education Institutions of China (Grant no. 14KJB150025), and the Qing Lan Project.

References

[1] G.-F. Huang, Z.-L. Ma, W.-Q. Huang et al., "Ag_3PO_4 semiconductor photocatalyst: possibilities and challenges," *Journal of Nanomaterials*, vol. 2013, Article ID 371356, 8 pages, 2013.

[2] Z. Yi, J. Ye, N. Kikugawa et al., "An orthophosphate semiconductor with photooxidation properties under visible-light irradiation," *Nature Materials*, vol. 9, no. 7, pp. 559–564, 2010.

[3] W. Yao, B. Zhang, C. Huang, C. Ma, X. Song, and Q. Xu, "Synthesis and characterization of high efficiency and stable Ag_3PO_4/TiO_2 visible light photocatalyst for the degradation of methylene blue and rhodamine B solutions," *Journal of Materials Chemistry*, vol. 22, no. 9, pp. 4050–4055, 2012.

[4] Z. Wang, L. Yin, Z. W. Chen, G. W. Zhou, and H. X. Shi, "Photodegradation of methyl orange using magnetically recoverable $AgBr@Ag_3PO_4/Fe_3O_4$ photocatalyst under visible light," *Journal of Nanomaterials*, vol. 2014, Article ID 150150, 6 pages, 2014.

[5] Z. Xiu, Y. Wu, X. Hao, Q. Lu, and S. Liu, "Graphene oxide wrapped Ag_3PO_4 sub-microparticles with highly enhanced photocatalytic activity and stability under visible light irradiation," *Materials Research Bulletin*, vol. 59, pp. 192–198, 2014.

[6] P. Dong, E. Cui, G. Hou, R. Guan, and Q. Zhang, "Synthesis and photocatalytic activity of $Ag_3PO_4/TiOF_2$ composites with enhanced stability," *Materials Letters*, vol. 143, pp. 20–23, 2015.

[7] Y. Bi, H. Hu, S. Ouyang, Z. Jiao, G. Lu, and J. Ye, "Selective growth of Ag_3PO_4 submicro-cubes on Ag nanowires to fabricate necklace-like heterostructures for photocatalytic applications," *Journal of Materials Chemistry*, vol. 22, no. 30, pp. 14847–14850, 2012.

[8] W. Liu, M. Wang, C. Xu, S. Chen, and X. Fu, "Ag_3PO_4/ZnO: an efficient visible-light-sensitized composite with its application in photocatalytic degradation of Rhodamine B," *Materials Research Bulletin*, vol. 48, no. 1, pp. 106–113, 2013.

[9] B. C. Cao, P. Y. Dong, S. Cao, and Y. H. Wang, "BiOCl/Ag_3PO_4 composites with highly enhanced ultraviolet and visible light photocatalytic performances," *Journal of the American Ceramic Society*, vol. 96, no. 2, pp. 544–548, 2013.

[10] P. Dong, Y. Wang, B. Cao et al., "Ag_3PO_4/reduced graphite oxide sheets nanocomposites with highly enhanced visible light photocatalytic activity and stability," *Applied Catalysis B: Environmental*, vol. 132-133, pp. 45–53, 2013.

[11] P. He, L. Song, S. Zhang, X. Wu, and Q. Wei, "Synthesis of g-C_3N_4/Ag_3PO_4 heterojunction with enhanced photocatalytic performance," *Materials Research Bulletin*, vol. 51, pp. 432–437, 2014.

[12] P. Hu, L. Yu, A. Zuo, C. Guo, and F. Yuan, "Fabrication of Monodisperse magnetite hollow spheres," *The Journal of Physical Chemistry C*, vol. 113, no. 3, pp. 900–906, 2009.

[13] P. Hu, X. Zhang, N. Han, W. Xiang, Y. Cao, and F. Yuan, "Solution-controlled self-assembly of ZnO nanorods into hollow microspheres," *Crystal Growth & Design*, vol. 11, no. 5, pp. 1520–1526, 2011.

[14] Y. Cao, J. Fan, L. Bai, F. Yuan, and Y. Chen, "Morphology evolution of Cu_2O from octahedra to hollow structures," *Crystal Growth & Design*, vol. 10, no. 1, pp. 232–236, 2010.

[15] Y. Bi, S. Ouyang, N. Umezawa, J. Cao, and J. Ye, "Facet effect of single-crystalline Ag_3PO4 sub-microcrystals on photocatalytic properties," *Journal of the American Chemical Society*, vol. 133, no. 17, pp. 6490–6492, 2011.

[16] P. Dong, J. Hu, Y. Huang, E. Cui, and G. Hou, "Synthesis of Ag_3PO_4 nanorods with enhanced photocatalytic activity," *Energy and Environment Focus*, vol. 4, pp. 1–5, 2015.

[17] H. Wang, Y. Bai, J. Yang, X. Lang, J. Li, and L. Guo, "A facile way to rejuvenate Ag_3PO_4 as a recyclable highly efficient photocatalyst," *Chemistry*, vol. 18, no. 18, pp. 5524–5529, 2012.

[18] Q. Liang, W. Ma, Y. Shi, Z. Li, and X. Yang, "Hierarchical Ag_3PO_4 porous microcubes with enhanced photocatalytic properties synthesized with the assistance of trisodium citrate," *CrystEngComm*, vol. 14, no. 8, pp. 2966–2973, 2012.

[19] Z.-M. Yang, Y.-Y. Liu, L. Xu, G.-F. Huang, and W.-Q. Huang, "Facile shape-controllable synthesis of Ag_3PO_4 photocatalysts," *Materials Letters*, vol. 133, pp. 139–142, 2014.

[20] X.-Z. Li, K.-L. Wu, C. Dong, S.-H. Xia, Y. Ye, and X.-W. Wei, "Size-controlled synthesis of Ag_3PO_4 nanorods and their high-performance photocatalysis for dye degradation under visible-light irradiation," *Materials Letters*, vol. 130, pp. 97–100, 2014.

[21] P. Dong, Y. Yin, N. Xu, R. Guan, G. Hou, and Y. Wang, "Facile synthesis of tetrahedral Ag_3PO_4 mesocrystals and its enhanced photocatalytic activity," *Materials Research Bulletin*, vol. 60, pp. 682–689, 2014.

[22] R. Asahi, T. Morikawa, T. Ohwaki, K. Aoki, and Y. Taga, "Visible-light photocatalysis in nitrogen-doped titanium oxides," *Science*, vol. 293, no. 5528, pp. 269–271, 2001.

[23] L. Zhu, X. Liu, J. Meng, and X. Cao, "Facile sonochemical synthesis of single-crystalline europium fluorine with novel nanostructure," *Crystal Growth and Design*, vol. 7, no. 12, pp. 2505–2511, 2007.

[24] J. H. Bang and K. S. Suslick, "Applications of ultrasound to the synthesis of nanostructured materials," *Advanced Materials*, vol. 22, no. 10, pp. 1039–1059, 2010.

[25] L. M. Miller, V. Vairavamurthy, M. R. Chance et al., "In situ analysis of mineral content and crystallinity in bone using infrared micro-spectroscopy of the ν_4 PO_4^{3-} vibration," *Biochimica et Biophysica Acta—General Subjects*, vol. 1527, no. 1-2, pp. 11–19, 2001.

[26] S. J. Gadaleta, E. P. Paschalis, F. Betts, R. Mendelsohn, and A. L. Boskey, "Fourier transform infrared spectroscopy of the solution-mediated conversion of amorphous calcium phosphate to hydroxyapatite: new correlations between X-ray diffraction and infrared data," *Calcified Tissue International*, vol. 58, no. 1, pp. 9–16, 1996.

[27] J. J. Liu, X. L. Fu, S. F. Chen, and Y. F. Zhu, "Electronic structure and optical properties of Ag_3PO_4 photocatalyst calculated by hybrid density functional method," *Applied Physics Letters*, vol. 99, no. 19, Article ID 191903, 2011.